Unraveling fungal endolysosomal network as a potential target for effective disease control

Xin Chen[1,2#], Xiaomin Chen[3#], Yunfei Long[1,2], Xiang Tian[1], Zhenyu Fang[1,2], Yakubu Saddeeq Abubakar[1,5], Huawei Zheng[4], Zonghua Wang[1,4*], Wenhui Zheng[1,2*]

[1] State Key Laboratory of Agricultural and Forestry Biosecurity, College of Plant Protection, Fujian Agriculture and Forestry University, Fuzhou, 350002 China;

[2] Key Laboratory of Bio-pesticide and Chemical Biology, Ministry of Education, College of Plant Protection, Fujian Agriculture and Forestry University, Fuzhou, 350002 China;

[3] Fujian University Key Laboratory for Plant Microbe Interaction, College of Life Sciences, Fujian Agriculture and Forestry University, Fuzhou 350002, China;

[4] Ministerial and Provincial Joint Innovation Centre for Safety Production of Cross-Strait Crops, College of Geography and Oceanography, Minjiang University, Fuzhou 350108, China;

[5] Department of Biochemistry, Faculty of Life Science, Ahmadu Bello University, Zaria 810281, Nigeria.

# These authors contributed equally to this work.

* Authors for correspondence:

Wenhui Zheng (wenhuiz@fafu.edu.cn), Zonghua Wang (wangzh@fafu.edu.cn).

Abstract

During host-pathogen interactions, fungal pathogens exploit the endolysosomal trafficking network to fine-tune their responses to host and environmental stimuli, thereby facilitating disease progression. However, the molecular mechanisms underlying the fungal-specific functions of the endolysosomal network require further investigation. Here, we systematically characterized the endolysosomal network in *Fusarium graminearum* using the dynamin-like GTPase FgVps1 as an entry point. Functional analysis revealed that FgVps1 is essential for the release of retromer- and sorting nexin-associated vesicles from endosomes, thereby facilitating the trafficking of v-SNARE protein FgSnc1 and promoting fungal development and pathogenicity. Building on this, we further discovered that the retromer core subunit FgVps35 interacts with sorting nexin FgSnx4 and identified the corresponding interaction interface, which involves residues FgVps35^{N383} and FgSnx4^{E373}. In addition, the ESCRT-II component FgVps36 bridges ESCRT-I and -III and interacts with both FgVps35 and FgSnx4, thereby preventing their mislocalization to the vacuole and maintaining endolysosomal trafficking. Notably, we demonstrated that inhibition of FgVps1 function, either by blocking its GTPase activity or by disrupting actin polymerization, effectively impaired endosomal trafficking and attenuates fungal pathogenicity. Altogether, our results uncover key mechanisms underlying the function of fungal endolysosomal network and providing a promising broad-spectrum strategy for controlling phytopathogenic fungi.

Introduction

Each year, crop losses due to emerging fungal pathogens pose a serious risk to global food security [1, 2]. Successful colonization of fungal pathogens requires not only the ability to evade or suppress host immune responses, but also tightly regulated coordination of intracellular processes that maintain cellular homeostasis and facilitate rapid adaptation to host physiological signals [3, 4]. Therefore, elucidating the cellular and molecular strategies that pathogens employ to coordinate homeostasis during host colonization is critical to understanding disease progression and developing effective control strategies.

A key role in maintaining cellular homeostasis under biotic and abiotic stress is played by the endolysosomal network, a highly dynamic transport system in eukaryotes that is spatially and temporally regulated [5]. Following endocytosis, cargo proteins are transported from the cell surface to the early endosomes, where the sorting process takes place. In this phase, cargos are either recycled or degraded [5, 6]. Recycling pathways include direct return of cargos to the plasma membrane or transit through the endocytic recycling compartment. In addition, some selected cargos can be retrieved into the trans-Golgi network to subsequently reach the cell surface via the secretory pathway. In contrast, cargos destined for degradation are sorted into intraluminal vesicles within the multivesicular bodies at the late endosomes, which subsequently fuse with vacuoles (or lysosomes in mammalian systems) to facilitate degradation [6, 7, 8]. This process is controlled by an evolutionarily conserved molecular machinery that includes Rab GTPases, retromer, sorting nexins and the ESCRT (Endosomal Sorting Complex Required for Transport) complex. Despite the conservation of these components across species, there are significant differences in gene copy number, functional specialization and regulatory complexity, reflecting species-specific requirements for endosomal transport and homeostatic control.

There is growing evidence for the importance of the endolysosomal network in the pathogenicity of plant-infecting fungi [9, 10]. Dysfunction of the endolysosomal network affects fungal development and the pathogenesis of various fungal pathogens [9, 10]. During host-pathogen interactions, components of the endolysosomal system modulate autophagy, a key process that enables fungal cells to adapt to metabolic changes and environmental stress [11, 12, 13, 14, 15]. Additionally, fungal

pathogens utilize the endolysosomal network to facilitate the secretion of effector proteins during host infection to suppress the host immune response [16, 17]. Furthermore, the endolysosomal network is closely associated with the production of mycotoxin, the toxic secondary metabolites that are toxic to plants and animals but contribute to the pathogen's ability to invade host tissues [18, 19, 20, 21, 22, 23, 24, 25]. Despite its crucial role, the molecular complexity of the endolysosomal network in fungal pathogens remains unclearly understood. In particular, the interplay between core trafficking components and other regulatory proteins within this system is yet to be fully elucidated.

In this study, we investigate the endolysosomal network in *Fusarium graminearum*, the causal agent of Fusarium head blight (FHB), to elucidate the molecular basis of endosomal trafficking during the pathogenesis of the fungus. By immunoprecipitation-mass spectrometry (IP-MS), we identified the dynamin-like GTPase FgVps1 as a common interactor of the sorting nexin FgSnx4 and the retromer core subunit FgVps35. Functional analyses revealed that FgVps1 is essential for endosomal sorting, with the v-SNARE protein FgSnc1 identified as one of its cargo proteins. By using FgVps1 as a regulatory nexus, we systematically analyzed the interactions between the core components of the endolysosomal network and elucidate the mechanisms controlling FgSnc1 transport. In addition to the conserved role of FgVps1 in vesicle release, we identified a fungal-specific interaction between FgSnx4 and FgVps35 and uncovered the crucial role of the ESCRT machinery in maintaining endosomal sorting homeostasis. Moreover, we found that phenothiazines selectively inhibit the GTPase activity of FgVps1 by binding the D239-I247 region of the protein, thereby impairing the fungal growth and pathogenicity. In addition to perturbing the GTPase activity of FgVps1, phenothiazine treatment also disrupts actin polymerization, leading to defects in endocytosis and vesicle trafficking. Collectively, these results provide insight into the complex interplay of the endolysosomal network in phytopathogenic fungi and lay a theoretical foundation for the development of environmentally friendly disease management strategies.

Results

FgVps1 is important for the development and pathogenicity of *F. graminearum*

We have previously pointed out the important role of the endolysosomal network in the development and pathogenicity of *F. graminearum*, the causal agent of wheat head blight (Fig. S1A)

124 [18, 19, 20, 22, 23, 24, 26, 27]. A highly enriched protein, FgVps1 (FGSG_07172), was identified by screening
125 the IP-MS data of the retromer core subunit FgVps35 and the sorting nexin FgSnx4. FgVps1 is a
126 dynamin-like GTPase that belongs to the dynamin superfamily. Structurally, FgVps1 contains three
127 domains: a GTPase (G) domain, a dynamin central region (DM) domain and a dynamin GTPase
128 effector (GED) domain (Fig. S1B). We also performed a phylogenetic analysis of the dynamin
129 superfamily proteins and found that FgVps1 is the only homolog of Vps1 involved in endocytic
130 vesicle scission in fungi (Fig. S1C). To further explore the biological functions of FgVps1, we
131 generated Δ*Fgvps1* mutants and confirmed the gene deletion by Southern blot assay (Fig. S2A). We
132 also generated a complemented strain Δ*Fgvps1*-com by expressing a vector harboring GFP-*FgVPS1*
133 into the Δ*Fgvps1* mutant (Fig. S2B). Phenotypic analyses revealed that the absence of FgVps1 leads
134 to severe defects in the vegetative growth, conidiation and sexual reproduction of the fungus (Fig.
135 S2C to S2F). In addition, compared to the wild type and the complemented strain, the virulence of
136 the Δ*Fgvps1* mutant was significantly reduced (Fig. 1A). Overall, these results indicate that FgVps1
137 loss-of-function perturbs *F. graminearum* development and pathogenicity.
138
139 **The Rab GTPases FgRab51 and FgRab7 regulate the intracellular dynamic of FgVps1**
140 To further decipher the mechanism of FgVps1 in relation to the development and pathogenicity of
141 the fungus, we performed GFP pull-down and subsequent tandem LC-MS/MS mass spectrometry
142 to identify potential FgVps1-associated proteins in *F. graminearum*. As shown in Fig. 1B and Table
143 S3, several proteins that are involved in endolysosomal sorting were detected and identified,
144 including Rab GTPases, the retromer complex and sorting nexins. Along the endolysosomal
145 network, Rab GTPases play a key role in cargo sorting and have been shown to be important for the
146 development and pathogenicity of *F. graminearum* [6, 27]. Using a Co-IP assay, we found that FgVps1
147 interacts with FgRab51 (Fig. 1C). To further confirm this association, we co-expressed mCherry-
148 FgVps1 with GFP-FgRab51 in the wild type. Through time-lapse imaging and further trajectory
149 analysis, we found that FgVps1 co-localized with the early endosomal marker FgRab51 (Fig. 1D),
150 consistent with the positive interaction earlier observed. Similar to FgRab51, Co-IP assay and
151 confocal microscopy showed that FgVps1 interacts with FgRab7 and co-localizes with FgRab7-
152 marked late endosomes (Fig. 1E and 1F).
153

154 To further investigate the association of FgVps1 with FgRab51 and FgRab7, we transformed a GFP-
155 FgVps1 vector into the Δ*Fgrab51* and Δ*Fgrab7* mutants. Time-lapse analysis revealed that the
156 trajectory length of FgVps1 was significantly reduced in both Δ*FgRab51* and Δ*FgRab7* mutants,
157 suggesting that the Rab GTPases FgRab51 and FgRab7 are required for the proper sub-cellular
158 dynamics of FgVps1 (Fig. 1G). To confirm this result, we conducted a fluorescence recovery after
159 photobleaching (FRAP) assay to monitor FgVps1 diffusion in the respective strains. As shown in
160 Fig. 1H, FgVps1 signal can be recovered by up to 60% within 30s after photobleaching in the wild
161 type, while in the Δ*Fgrab51* and Δ*Fgrab7* mutants, only 40% fluorescence recovery rate was
162 observed. These results demonstrate that the intracellular dynamics of FgVps1 are impaired in the
163 absence of FgRab51 and FgRab7.
164
165 In yeast, Mvp1 was shown to recruit Vps1 to the endosomes [28, 29, 30]. However, in *F. graminearum*,
166 Δ*Fgmvp1* mutant displayed some phenotypic differences with Δ*Fgvps1* [29, 31]. As shown above, the
167 Rab GTPases contribute to the proper dynamics of FgVps1. Previous studies also demonstrated that
168 Rab GTPases are required for the recruitment of the retromer complex (a protein sorting machinery)
169 and sorting nexins to the endosomes [16, 19, 26, 32]. Therefore, we proposed that FgRab51 and FgRab7
170 mediate the recruitment of FgVps1 to the endosomes in *F. graminearum*. To test this hypothesis,
171 we stained the strains expressing GFP-FgVps1 fusion protein with FM4-64 dye to visualize the
172 endosomal structures. Time-lapse imaging revealed that FgVps1 is closely associated with FM4-
173 64-labeled endosomes in the wild-type strain, contrary to their segregated distribution in the
174 Δ*Fgrab51* and Δ*Fgrab7* mutants (Fig. S3). Together with the FRAP assay data, these results further
175 support the important role of Rab GTPases FgRab51 and FgRab7 in maintaining FgVps1 dynamic
176 during endosomal maturation.
177
178 **FgVps1 is required for endosomal sorting of FgSnc1**
179 Endocytic cargos travel via the endolysosomal pathway to endosomes where their fate is determined
180 [5]. Although we have established that FgVps1 is localized to endosomes, its function at the
181 endosomes remains unclear in *F. graminearum*. When screening the FgVps1 IP-MS data, we found
182 that both FgSnx4 and its cargo FgSnc1 were present in the FgVps1 interactome (Fig. 2A, Table S3).
183 Similar to the Δ*Fgsnx4* and Δ*Fgsnc1* mutants, the loss of FgVps1 showed a defect in hyphal

184 morphogenesis (Fig. 2B). Further time-lapse imaging revealed that FgVps1 is closely associated
185 with FgSnc1 in growing hyphae (Fig. 2C). To further confirm the role of FgVps1 in the sorting of
186 FgSnc1, a FRAP assay was performed to investigate the possible diffusion of FgSnc1 in the two
187 mutants Δ*Fgsnx4* and Δ*Fgvps1*. As shown in Fig. 2D, 50% of the FgSnc1 signal in the wild type
188 can be recovered within 1 min after photobleaching, while only 20% fluorescence recovery was
189 observed in the Δ*Fgvps1* and Δ*Fgsnx4* mutants. Furthermore, we also analyzed the localization of
190 FgSnc1 in basal hyphae. Unlike its localization to the plasma membrane in the wild type, FgSnc1
191 was observed to be mis-localized to the vacuole in both Δ*Fgsnx4* and Δ*Fgvps1* mutants (Fig. 2E).
192 Consistently, western blot assay also showed that the GFP-FgSnc1 band degradation rate was
193 significantly increased in Δ*Fgvps1* and Δ*Fgsnx4* mutants (Fig. 2F). Overall, these results indicate
194 that FgVps1 is required for proper endosomal sorting of FgSnc1.
195
196 **FgVps1 is indispensable for the endosomal discharge of FgVps35 and FgSnx4**
197 In *F. graminearum,* both FgVps35 and FgSnx4 contribute to endosomal sorting of FgSnc1 [19, 33]. To
198 further investigate the role of FgVps1 in the sorting of FgSnc1, Co-IP assay was performed to check
199 for possible interaction between FgVps1 and FgVps35, as well as between FgVps1 and FgSnx4. As
200 shown in Fig. S4A, FgVps1 can interact with FgVps35 and FgSnx4 *in vivo*. Similar to FgVps35 and
201 FgSnx4, FgVps1 can also interact with FgSnc1 (Fig. S4B). Consistent with this, confocal
202 examination also showed that the dynamics of FgVps1 are closely associated with FgVps35 and
203 FgSnx4 (Fig. 3A). Further analysis of the IP-MS data of FgVps1, FgVps35 and FgSnx4 revealed
204 that these proteins share many potential interaction partners (Fig. 3B). Previously, Vps1 was
205 reported to mediate the scission of endosomal tubules in yeast [30]. To test whether this holds true in
206 *F. graminearum*, we transformed FgSnx4-GFP and FgVps35-GFP vectors into the wild type and
207 the Δ*Fgvps1* mutant. We found that, unlike the wild type, FgVps35 and FgSnx4 were trapped in
208 some speckled structure in the tips and in elongated tubules of the fungal basal hyphae, suggesting
209 the conserved roles of FgVps1 in the endosomal discharge of retromer (FgVps35) and the sorting
210 nexin FgSnx4 (Fig. 3C).
211
212 To exert its function, retromer interacts with various sorting nexins, including Snx1/2, Snx3, Snx5/6
213 and Snx27 [34, 35]. However, *F. graminearum* does not have a homolog of Snx27. Moreover, Δ*Fgsnx3*

214 mutant showed phenotypes that are different from those of retromer mutant [31]. Given that FgSnx4
215 had similar interactome to FgVps35, we hypothesized that FgVps35 and FgSnx4 may interact to
216 jointly execute their biological functions. To test this hypothesis, yeast two-hybrid and Co-IP assays
217 were carried out to check for possible interaction between FgVps35 and FgSnx4. As shown in Fig.
218 3D and 3E, FgVps35 directly interacts with FgSnx4 both *in vivo* and *in vitro*. To further validate
219 the association of FgVps35 and FgSnx4, an *in silico* interaction model of FgVps35 and FgSnx4 was
220 analyzed using AlphaFold2. As shown in Fig. 3F, the asparagine residue N383 of FgVps35 was
221 observed to interact with the glutamate residue E373 of FgSnx4 via hydrogen bonding. Sequence
222 alignment further revealed that the E373 of FgSnx4 is evolutionarily conserved across species, and
223 that both E and threonine (T) residues at this position are capable of forming hydrogen bonds,
224 whereas the N383 site appears to be fungi-specific (Fig. S5). To validate this prediction, we
225 disrupted this hydrogen bond by introducing N383A and E373A point mutations in FgVps35 and
226 FgSnx4, respectively, and then analyzed the mutated proteins for possible interaction by yeast two-
227 hybrid (Y2H) assay. We found a weakened interaction between FgVps35 and FgSnx4 due to N383A
228 mutation, and the interaction was completely abolished following E373A mutation. Moreover,
229 pathogenicity tests on wheat heads revealed that the FgSnx4 E373A mutation caused reduced
230 virulence compared to the wild type (Fig. 3G). These results suggest that the FgSnx4 E373 residue
231 is important for the interaction of FgSnx4 with FgVps35.
232
233 **The ESCRT complex ensures the continuous sorting of FgSnc1**
234 Previous studies indicated that ubiquitination of Snc1 is crucial for its recycling [36, 37]. However,
235 although the ubiquitination site of Snc1 remains conserved in *F. graminearum* (Fig. S6 A), mutation
236 of K65 residue of FgSnc1 has no significant effect on the recycling of the protein and does not affect
237 the growth of the fungus, indicating that the FgSnc1 K65 site is not necessary for the sorting of
238 FgSnc1 (Fig. S6 B to E). Within the endosomal network, the ESCRT complex plays a key role in
239 protein degradation and vesicle budding [7, 38]. Similar to the retromer and sorting nexins, the ESCRT
240 machinery is also required for fungal development and pathogenicity in *F. graminearum* [22, 23, 24].
241 Given that ubiquitination of FgSnc1 at the conserved K65 site appears to be dispensable for its
242 recycling and fungal growth, we speculated that FgSnc1 sorting might instead be regulated by
243 alternative mechanisms. Therefore, we hypothesized that the ESCRT complex could function as a

244 potential regulator of FgSnc1 sorting by interacting with its associated sorting machinery. We first
245 investigated the interaction of ESCRT complex with the retromer core component FgVps35 and the
246 sorting nexin FgSnx4. We found that FgVps35 and FgSnx4 positively interact with several
247 components of the ESCRT complex (Fig. 4A). Among them, the ESCRT-II component FgVps36
248 physically interacts with both FgVps35 and FgSnx4 and serves as a bridge linking ESCRT-I and
249 ESCRT-III (Fig. 4A and 4B). Through CMAC staining (for visualization of vacuole lumen), we
250 found that loss of *FgVPS36* disrupts the endolysosome homeostasis, with more vacuoles observed
251 in both hyphal tips and basal hyphae (Fig. 4C). In addition, compared to the wild type, more band
252 degradation of the endolysosomal components (including FgVps35, FgSnx4, FgVps1 and FgSnc1)
253 was observed in Δ*Fgvps36* mutant (Fig. 4D). Consistent with this observation, live cell imaging
254 showed that FgVps35 and FgSnx4 are mis-localized to the vacuole in Δ*Fgvps36* mutant (Fig. 4E
255 and 4F). We also expressed GFP-FgSnc1 in the Δ*Fgvps36* mutant to analyze its subcellular
256 distribution. Unlike its plasma membrane localization in the wild type, FgSnc1 was highly
257 accumulated in the vacuole in the Δ*Fgvps36* mutant (Fig. 4G to 4I). Altogether, our results indicate
258 that the ESCRT component FgVps36 interacts with the retromer and sorting nexin to modulate the
259 cellular homeostasis of FgSnc1.
260
261 **Phenothiazine treatment inhibits FgVps1 GTPase activity and subsequent FgSnc1 sorting**
262 In contrast to other species, Vps1 is the only protein of the dynamin superfamily that is used by
263 phytopathogenic fungi for endocytic transport[39]. To determine whether inhibition of FgVps1 could
264 serve as a potential disease control strategy, the phenothiazine derivatives chlorpromazine (CPZ)
265 and prochlorperazine (PCZ) were used for further treatment. Phenothiazines, a clinically used
266 antipsychotic, exhibits dynamin inhibitory activity, but its effect on phytopathogens remains largely
267 unexplored [40, 41]. As shown in Fig. S7A, treatment with phenothiazines can significantly impair the
268 growth of *F. graminearum*. We also investigated the effects of phenothiazines on plant infection. In
269 particular, when treated with CPZ and PCZ, *F. graminearum* showed severe defects in invasive
270 growth and virulence on wheat coleoptiles (Fig. S7B and S7C). Since phenothiazines were
271 previously shown to inhibit dynamin GTPase activity, we further purified the recombinant GST-
272 FgVps1 protein and incubated it with phenothiazines for 30 min. Subsequent GTPase activity assay
273 indicated that the FgVps1 GTPase activity was significantly reduced under phenothiazines treatment,

274 indicating the conserved role of phenothiazines in inhibiting the GTPase activity of dynamins (Fig.
275 5A). In addition, treatment with phenothiazines compromised the normal intracellular distribution
276 of FgVps1 and disrupted the intracellular trafficking of FgSnc1 (Fig. 5B and 5C).
277
278 As a typical protein of the dynamin superfamily, FgVps1 contains three domains: G-domain
279 (GTPase domain), DM (dynamin central region) and GED (dynamin GTPase effector domain) (Fig.
280 S1B). By mutating the domains, we found that these domains all contribute to the full function and
281 subcellular distribution of FgVps1 (Fig. 5D and S8A). To further identify the structural basis of
282 FgVps1 association with phenothiazines, we constructed the molecular docking model of FgVps1
283 with the phenothiazines CPZ and PCZ using AutoDock [42]. Interestingly, among the different binding
284 pockets identified, CPZ and PCZ share the same binding pocket with FgVps1, which consists of
285 amino acids from D239 to I247 (Fig. S8B). The binding pocket for phenothiazines belongs to the G
286 domain, which is involved in the binding and hydrolysis of GTP [39]. To determine whether this
287 binding pocket is functionally important for the GTPase activity of FgVps1, we generated a
288 truncated FgVps1 protein lacking this pocket (FgVps1$^{\Delta POC}$, deletion of residues D239-I247).
289 Subsequently, we purified the recombinant GST-FgVps1$^{\Delta POC}$ protein and analyzed its GTPase
290 activity in vitro (Fig. S8C). As shown in Fig. 5E, the mutation of the binding pocket caused a
291 significant reduction in the GTPase activity of FgVps1. Also, loss of the phenothiazines binding
292 pocket impairs the full function of FgVps1 (Fig. 5F and 5G). Consistent with *FgVPS1* deletion and
293 G domain mutation, loss of the phenothiazines binding pocket disrupted the proper FgSnc1 sorting
294 (Fig. 5H). Taken together, these findings suggest that inhibiting the GTPase activity of FgVps1,
295 either by genetic or chemical means, significantly impairs the development and pathogenicity of *F.*
296 *graminearum*.
297
298 **Treatment of phenothiazines impaired actin polymerization in phytopathogenic fungi**
299 It was noted that treatment of *F. graminearum* with a high concentration of phenothiazines
300 (100 μg/mL) caused more severe defects than those observed in the *FgVPS1* deletion mutant,
301 suggesting that apart from disruption of FgVps1 activity, phenothiazines affect additional cellular
302 processes. Considering the central role of actin in promoting cell polarity and vesicle trafficking [43],
303 we speculated that phenothiazines could interfere with actin organization. To check this, we treated

304 a strain expressing GFP-FgSnc1 with phenothiazines or the actin polymerization inhibitor
305 Latrunculin A (Lat A). As shown in Fig. S9A, both treatments disrupted the polarized localization
306 of FgSnc1. We further assessed the effect of phenothiazines on actin organization and found that
307 actin localization at the Spitzenkörper was markedly reduced, indicating disrupted polymerization
308 (Fig. 6A). Since actin organization is also crucial for endocytosis in filamentous fungi, we
309 investigated the effects of phenothiazines on this process using FM4-64 dye. In the control hyphae
310 (treated with DMSO), FM4-64 clearly labeled the vacuolar membrane within 25 min. In contrast,
311 FM4-64 was observed to accumulate in the cytosol in the phenothiazine-treated hyphae, indicating
312 delayed endocytosis (Fig. 6B). To further validate these observations, we monitored the
313 internalization of the uric acid-xanthine permease FgUapC [27]. During growth in MM-N medium
314 containing 5 μM urea, FgUapC mainly localized to the plasma membrane. Upon switching to an
315 ammonium-containing medium (10 μM NH_4Cl), FgUapC was internalized and delivered to the
316 vacuole in the control cells. However, in phenothiazine-treated hyphae, FgUapC remained localized
317 at the plasma membrane even after 3.5 hours, indicating a delay in endocytic trafficking (Fig. 6C).
318
319 Given the important role of actin in vesicle trafficking in filamentous fungi[43], we then investigated
320 whether actin organization influences FgVps1 dynamics. In a strain co-expressing GFP-FgRab7 and
321 mCherry-FgVps1, Lat A treatment did not alter the endosomal localization of FgVps1 but
322 significantly reduced its dynamic movement as indicated by shorter tracking trajectories (Fig. 6D).
323 To determine whether these effects are conserved across phytopathogenic fungi, we treated
324 *Magnaporthe oryzae* with the phenothiazine derivatives. Consistent with the findings in *F.*
325 *graminearum*, treatment of *M. oryzae* with the drugs caused defects in the fungal development and
326 pathogenicity (Fig. S9B). Moreover, treatment with CPZ disrupted actin polymerization in *M.*
327 *oryzae* (Fig. 6E). We also treated other phytopathogenic fungi, including *Fusarium oxysporum*,
328 *Fusarium verticillioides*, *Colletotrichum graminicola*, *Rhizoctonia solani*, *Sclerotinia sclerotiorum*,
329 and *Botrytis cinerea* with the drugs and observed similar growth inhibition effect across these
330 species. Collectively, these results indicate that phenothiazines exert antifungal activity not only by
331 impairing FgVps1-mediated vesicle trafficking but also by disrupting actin polymerization and
332 subsequent endocytosis, ultimately compromising fungal growth and virulence.
333

334 **Discussion**

335 Accumulating evidence has highlighted the crucial role of endolysosomal network in maintaining
336 cellular homeostasis and its close association with the development and pathogenesis of
337 phytopathogenic fungi [5, 10]. However, the intricate mechanisms regulating this network and its
338 potential for fungal disease control remains limited. In this study, we identified the dynamin-like
339 GTPase FgVps1 as a molecular "scissor" functioning in the endosomal network. FgVps1 is first
340 recruited to endosomes by the Rab GTPases FgRab51 and FgRab7, where it facilitates the release
341 of vesicles containing the retromer and sorting nexins. The efficiency of this process is further
342 regulated by the ESCRT complex interacts directly with FgVps35 and FgSnx4. Importantly,
343 disruption of endosomal sorting, either by inhibiting FgVps1 activity or blocking actin
344 polymerization, significantly compromised the growth and virulence of *F. graminearum* (Fig. 7).
345 These findings unveil new insights into the functions of the endolysosomal system and suggest a
346 potentially promising strategy for phytopathogenic fungal disease control.

347

348 Dynamins are multi-domain GTPases involved in multiple membrane remodeling processes
349 (including scission and fusion of endocytic vesicles and organelles) and cell division events [39, 44, 45].
350 Unlike the many dynamin proteins identified in mammals and plants [39, 44], fungi contain only three
351 dynamin proteins namely Dnm1, Vps1 and Sey1; Dnm1-dependent mitochondrial fission and Sey1-
352 mediated ER fusion have been shown to be important for the development, fungicide resistance and
353 pathogenicity of phytopathogens [46, 47, 48]. Although Vps1 has previously been linked to endocytosis,
354 vesicle scission and peroxisome fission and recycling [29, 30, 49, 50, 51, 52], its precise roles in fungal
355 phytopathogens remain poorly understood. In this study, we demonstrated that FgVps1 plays a
356 conserved role in vesicle release and provided compelling evidence that its function and dynamics
357 are dependent on Rab GTPases and proper actin organization (Fig. 1, Fig. 3, and Fig. 6). Previous
358 studies in yeast have shown that the endosomal recruitment of Vps1 depends on Mvp1, which
359 facilitates the release of recycling tubules [28, 29, 30]. However, in *F. graminearum*, there are clear
360 phenotypic differences between Δ*Fgmvp1* and Δ*Fgvps1* mutants [31], suggesting that FgVps1 exerts
361 its functions independent of FgMvp1. Our results demonstrated that the Rab GTPases FgRab51 and
362 FgRab7 contribute to the endosomal recruitment of FgVps1 and are essential for maintaining its
363 intracellular dynamics (Fig. 1 and Fig. S3). FgVps1 function, Rab GTPases also play a conserved

364 role in recruiting sorting nexins and the retromer to endosomes, thereby coordinating the endosomal
365 sorting process [19, 26, 32, 53]. The functional diversity of Rab GTPases reflects an evolutionary
366 adaptation that ensures precise regulation of endosomal trafficking during pathogenic fungal
367 development and host colonization. Additionally, our findings demonstrate that proper actin
368 organization also contributes to the dynamic of FgVps1 (Fig. 6). Given the crucial role of actin in
369 both endocytosis and vesicle trafficking [5, 43, 54], disrupting endolysosomal homeostasis by interfering
370 with fungus-specific actin-driven vesicle motility may offer a promising strategy for fungal disease
371 management.
372
373 Moreover, we also systematically characterized the role of FgVps1 in endosomal sorting using
374 FgSnc1 as a representative cargo. Intriguingly, we found that FgSnx4 and FgVps35 are trapped in
375 the same endosomal tubule in Δ*Fgvps1* mutant (Fig. 3C). Further analysis revealed that FgSnx4
376 directly interacts with FgVps35 through the E737 residue of the former (Fig. 3F). Previous studies
377 in yeast and mammals demonstrated that the retromer interacts with different sorting nexins to
378 modulate cargo sorting [35, 55]; however, some of those sorting nexins are either absent or their loss-
379 of-function displays different phenotypes in phytopathogens. The observed interaction between
380 FgSnx4 and FgVsps35 may thus represent an evolved adaptation in phytopathogens to optimize
381 intracellular trafficking for successful host colonization. To better understand the specialized
382 endosomal sorting mechanisms in these pathogens, we attempted to investigate the relationship
383 between the FgSnx4-FgVps35 heterodimer and the ESCRT complex. We found that the ESCRT
384 complex is crucial for proper cargo sorting and directly interacts with both FgSnx4 and FgVps35 to
385 maintain endosomal homeostasis (Fig. 4). Interestingly, unlike the compartmentalized network seen
386 in yeast and mammals, the endosomal system in fungal pathogens appears to be structurally "coarse"
387 yet functionally efficient. This functional robustness is likely achieved through the tight interplay
388 of Rab GTPases (Rab5 and Rab7), dynamin (FgVps1), sorting machineries (retromer and sorting
389 nexins) and the ESCRT complex (Fig.1, Fig. 3 and Fig. 4) [19, 26, 29, 31, 56]. Together, these findings
390 provide new insights into the role of the endolysosomal network in phytopathogens and its
391 contribution to fungal development and host infection.
392
393 The antipsychotic drugs phenothiazines exhibit antimicrobial effects against human pathogenic

394 bacterial and fungi [41, 57, 58]. Previous studies indicated that phenothiazines interfere with calcium-
395 calmodulin system, membrane stabilization and efflux pumps to strive an antifungal effect [59, 60]. In
396 this study, we provide new evidence that phenothiazines exert antifungal effects by compromizing
397 the function of the endolysosomal network. Specifically, phenothiazines target and bind to D239-
398 I247 amino acid residues in the GTPase (G) domain of FgVps1, thereby inhibiting its GTPase
399 activity and disrupting FgVps1-associated endosomal sorting (Fig. 5). In parallel, phenothiazine
400 treatment interferes with actin polymerization in phytopathogenic fungi, leading to defects in
401 polarity establishment and endocytosis. This disruption also impairs the intracellular dynamics of
402 FgVps1, further compromising endolysosomal trafficking (Fig. 6). To facilitate host colonization,
403 many pathogens manipulate the host's endolysosomal system to enhance their colonization
404 efficiency [61, 62, 63, 64]. it is plausible that phenothiazines may also inhibit pathogen entry by targeting
405 host endocytosis. Since phenothiazines are synthetic drugs with diverse biological activities [57],
406 further understanding of their mechanism of action may be promising for effective drug
407 development and repurposing.
408
409 **Materials and methods**
410 **Fungal strains and culture conditions**
411 The PH-1 strain of *F. graminearum* was used as the wild type. A list of all the strains used in this
412 study is provided in Table S1. The strains were cultured as previously described [18]. In brief, the *F.*
413 *graminearum* strains were cultured on CM and CMC media for growth and conidia production,
414 respectively.
415 To assess the impact of phenothiazines on the indicated fungal pathogens, *Fusarium oxysporum*
416 (FocTR4) and *Fusarium verticillioides* (7600) were inoculated on CM media, while *Colletotrichum*
417 *graminicola* (M1.001), *Rhizoctonia solani* (GD118), *Sclerotinia sclerotiorum* (1980 UF-70) and
418 *Botrytis cinerea* (B05.10) were inoculated on CMII media (10 g/L glucose, 2 g/L peptone, 1 g/L
419 yeast extract, 1 g/L casamino acid, 5% (v/v) nitrate salts, 0.1% (v/v) trace elements and 0.1% (v/v)
420 vitamin solution). After inoculation, all strains were incubated at 28 °C under dark condition.
421
422 **Generation of *FgVPS1* gene deletion mutants and complementation**
423 For the generation of Δ*Fgvps1* mutants, split-marker approach was used as described previously [65].

424 Briefly, approximately 1kb upstream and downstream sequences of *FgVPS1* gene were amplified
425 using specific primer pairs (Table S2). The resulting fragments were then fused with hygromycin
426 resistance gene cassette through splicing by overlap extension (SOE) PCR and then transformed
427 into the wild type PH-1 protoplasts. The resulting transformants were screened by PCR and further
428 confirmed by Southern blot assay. For *FgVPS1* complementation, a GFP-Fgvps1 vector was
429 transformed into the Δ*Fgvps1* mutant protoplasts and, subsequently, positive transformants were
430 screened by GFP fluorescence detection using a confocal microscope as described below.
431 Additionally, the selected transformants were further verified through phenotypic assays.
432
433 **Plant infection assays**
434 For *F. graminearum* infection on wheat coleoptiles, conidia suspensions (10^6 spores/mL) of the
435 indicated strains were inoculated on wheat coleoptiles for 7 days as previous descripted [66]. For
436 pathogenicity on wheat heads, mycelial plugs of the related strains were inoculated into flowering
437 wheat heads for 14 days as previously descripted [18]. To monitor invasive growth, conidia
438 suspensions were injected into wheat coleoptiles and incubated in the dark for 3 days, under humid
439 condition at 28 °C, and then observed under a confocal microscope.
440 For *M. oryzae* pathogenicity assays on barley, conidia suspensions (5×10^4 conidia/mL) were drop-
441 inoculated onto barley leaves with or without phenothiazine treatment and incubated for 5 days, as
442 previously described [65].
443
444 **Confocal microscopy and analysis**
445 For monitoring endocytosis, hyphae of the fungal strains were incubated with 10 μg/mL FM4-64
446 dye (Cat. T3166, Invitrogen, Carlsbad, California) for 2 and 25 minutes, respectively. To stain the
447 vacuoles, hyphae of the indicated strains were treated with 50 μM CMAC (Cat. A6520, Invitrogen,
448 Carlsbad, California) for 30 min and then observed under a confocal microscope. For the disruption
449 of action polymerization, Latrunculin A (Lat A) was used at a final concentration of 5 μg/mL and
450 observed by confocal microscopy. All confocal microscopy examinations were performed using a
451 Nikon CSU-W1 spinning disk confocal microscope (Nikon, Japan). The excitation and emission
452 wavelengths used were 488 nm/500-550 nm for GFP and 561 nm/570-620 nm for mCherry as
453 previously descripted [16].

454 For statistical analysis of localization differences, data were collected from 30 hyphae per biological
455 replicate across three independent replicates. For the analysis of vesicle motion, time-lapse image
456 stacks were processed using Fiji [67]. Maximum intensity projections (MIPs) were generated from the
457 image stack to visualize the vesicle trajectory across the time series. Single-particle tracking analysis
458 was then performed using a TrackMate plugin. The net displacement of individual vesicles was
459 calculated as the straight-line distance between their initial and final positions, based on the
460 trajectories obtained from the single-particle tracking.
461
462 **Immunoprecipitation-mass spectrometry**
463 For the immunoprecipitation-mass spectrometry assays, the wild type strain PH-1 and the strains
464 expressing GFP and GFP-FgVps1 were cultured in liquid CM for two days. Mycelia were harvested,
465 ground into fine powder and then incubated in lysis buffer containing 2 mM PMSF and protease
466 inhibitor cocktail (Cat. GRF101, Epizyme Biotech, Shanghai, China) for 30 min. The samples were
467 centrifuged at 12,000 rpm for 20 minutes. Total cell lysates were further incubated with 30 μL GFP-
468 Trap A beads (Cat. gta-20; ChromoTek Inc., Planegg Martinsried, Germany) for 4 hours and then
469 heated at 100°C with protein loading buffer (Cat. LT103, Epizyme Biotech, Shanghai, China) for
470 10 minutes. Finally, the samples were separated by SDS-PAGE, and mass spectrometry analysis
471 was conducted to identify the related proteins bound to the GFP-FgVps1.
472
473 **Yeast two hybrid and co-immunoprecipitation (Co-IP) assays**
474 For yeast two hybrid assays, the CDS sequence of the various genes were amplified using the
475 specific primers listed in Table S2. The amplified sequences were cloned into pGADT7 or pGBKT7
476 vector and further verified by sequencing (Sangon biotech, Shanghai, China). The resulting vectors
477 were transformed into yeast strain AH109 according to Matchmaker™ GAL4 Two-Hybrid System
478 3 protocol (Clontech, Mountain View, CA, USA).
479 For Co-IP assay, the strains expressing the fusion proteins were inoculated in liquid CM at 28°C,
480 110 rpm for 36 h. The samples were collected and ground into fine powder in liquid nitrogen, and
481 then lysed in lysis buffer. The total cell lysates were then incubated with GFP-Trap A beads at 4 °C
482 for 4 h. The bound proteins were subsequently eluted by heating at 100°C for 10 min with protein
483 loading buffer and further analyzed by western blot using anti-GFP (Cat. M20004M, Abmart,

484 Shanghai, China) and anti-Myc (Cat. ab1326, Abcam, Cambridge, United Kingdom) antibodies.

485

486 **Phylogeny analysis, protein structure modeling and molecular docking**

487 For phylogeny analysis, the sequences of the dynamin proteins were downloaded from the NCBI
488 database (https://www.ncbi.nlm.nih.gov/). Phylogenetic tree was constructed by Neighbor-joining
489 method using MEGA-X and further modified using iTOL [68]. The protein structures of FgVps1 and
490 FgVps35-FgSnx4 multimer were predicted using AlphaFold2 [69] and further visualized using
491 PyMOL. The structures of prochlorperazine and chlorpromazine were downloaded from the NCBI
492 PubChem database and molecular docking of FgVps1 with the prochlorperazine and
493 chlorpromazine was performed using AutoDock and visualized by PyMOL.

494

495 **Protein purification and GTPase activity assay**

496 For the purification of GST-FgVps1 and GST-FgVps1$^{\Delta POC}$ recombinant proteins, the CDS
497 sequences of *FgVPS1* and *FgVPS1*$^{\Delta POC}$ were amplified using the specific primers listed in Table S2
498 and then cloned into pGET-4T-2 vector. The resulting vectors were expressed in *Escherichia coli*
499 BL21 cells and further sonicated in lysis buffer (150 mM NaCl, 50 mM Tris HCL, pH 8.0, 10%
500 glycerol) containing 2 mM PMSF and protease inhibitor cocktail (Cat. GRF101, Epizyme Biotech,
501 Shanghai, China). After sonication, the suspensions were centrifuged at 4 ℃, 12000rpm for 20 min
502 and incubated with GST beads (Cat. A10018, Abmart, Shanghai, China) for 2 h. The beads were
503 then washed with the washing buffer and eluted by incubating in an elution buffer (150 mM NaCl,
504 50 mM Tris HCL, pH 8.0, 150 mM glutathione) at 4 ℃ for 2 h.

505 To investigate the effects of phenothiazines on FgVps1 GTPase activity, the purified GST-FgVps1
506 was incubated with the different phenothiazines for 30 min and then the GTPase activity was
507 measured using a GTPase assay kit (Cat. ab272520, Abcam, Cambridge, United Kingdom) and
508 Tristar² S LB 942 multimode reader (Berthold, Germany). To check the effect of mutating the
509 binding pocket of FgVps1 on its GTPase activity, the purified GST-FgVps1 and GST-FgVps1$^{\Delta POC}$
510 proteins were quantified using a Bradford Protein Assay Kit (Cat. P0006C, Beyotime, Shanghai,
511 China) and then the GTPase activity was measured using a GTPase assay kit. GST was used for the
512 negative control. Data were collected from three biological repeats.

513

Author contributions

Conceptualization, ZHW and WHZ; methodology, XC, XMC and WHZ; investigation, XC, XMC, YFL，XT and ZYF; visualization, XC, ZHW and WHZ; Writing – Original Draft, XC; Writing – Review & Editing, XC, XMC, YSA, HWZ, ZHW and WHZ; resources and funding acquisition, XMC and WHZ. XC and XMC contributed equally to this work.

Acknowledgements

This research was supported by the National Natural Science Foundation of China (32272481, 32122071), the Postdoctoral Fellowship Program of CPSF (GZC20230448). The authors declared no financial or other potential conflict of interest.

References

1. Fones HN, Bebber DP, Chaloner TM, Kay WT, Steinberg G, Gurr SJ. Threats to global food security from emerging fungal and oomycete crop pathogens. *Nat Food* **1**, 332-342 (2020).

2. Dean R*, et al.* The Top 10 fungal pathogens in molecular plant pathology. *Mol Plant Pathol* **13**, 414-430 (2012).

3. van der Does HC, Rep M. Adaptation to the Host Environment by Plant-Pathogenic Fungi. *Annu Rev Phytopathol* **55**, 427-450 (2017).

4. Wang Y, Pruitt RN, Nurnberger T, Wang Y. Evasion of plant immunity by microbial pathogens. *Nat Rev Microbiol* **20**, 449-464 (2022).

5. Cullen PJ, Steinberg F. To degrade or not to degrade: mechanisms and significance of endocytic recycling. *Nat Rev Mol Cell Biol* **19**, 679-696 (2018).

6. Borchers AC, Langemeyer L, Ungermann C. Who's in control? Principles of Rab GTPase activation in endolysosomal membrane trafficking and beyond. *J Cell Biol* **220**, e202105120 (2021).

7. Migliano SM, Wenzel EM, Stenmark H. Biophysical and molecular mechanisms of ESCRT functions, and their implications for disease. *Curr Opin Cell Biol* **75**, 102062 (2022).

8. Posor Y, Jang W, Haucke V. Phosphoinositides as membrane organizers. *Nat Rev Mol Cell Biol* **23**, 797-816 (2022).

9. Shoji JY, Kikuma T, Kitamoto K. Vesicle trafficking, organelle functions, and unconventional

552 secretion in fungal physiology and pathogenicity. *Curr Opin Microbiol* **20**, 1-9 (2014).
553
554 10. Abubakar YS, Sadiq IZ, Aarti A, Wang Z, Zheng W. Interplay of transport vesicles during plant-
555 fungal pathogen interaction. *Stress Biol* **3**, 35 (2023).
556
557 11. Sun L*, et al.* A subunit of ESCRT-III, MoIst1, is involved in fungal development, pathogenicity,
558 and autophagy in Magnaporthe oryzae. *Front Plant Sci* **13**, 845139 (2022).
559
560 12. Sun LX*, et al.* Endosomal sorting complexes required for transport-0 (ESCRT-0) are essential
561 for fungal development, pathogenicity, autophagy and ER-phagy in Magnaporthe oryzae.
562 *Environ Microbiol* **24**, 1076-1092 (2022).
563
564 13. Zheng W*, et al.* Retromer is essential for autophagy-dependent plantinfection by the rice blast
565 fungus. *PLoS Genet* **11**, e1005704 (2015).
566
567 14. Liu XH*, et al.* The small GTPase MoYpt7 is required for membrane fusion in autophagy and
568 pathogenicity of Magnaporthe oryzae. *Environ Microbiol* **17**, 4495-4510 (2015).
569
570 15. Li B, Mao HY, Zhang ZY, Chen XJ, Ouyang SQ. FolVps9, a guanine nucleotide exchange factor
571 for FolVps21, is essential for fungal development and pathogenicity in Fusarium oxysporum f.
572 sp. lycopersici. *Front Microbiol* **10**, 2658 (2019).
573
574 16. Chen X*, et al.* Rab7/Retromer-based endolysosomal trafficking is essential for proper host
575 invasion in rice blast. *New Phytologist* **239**, 1384-1403 (2023).
576
577 17. Chen X*, et al.* Vacuolar recruitment of retromer by a SNARE complex enables infection-related
578 trafficking in rice blast. *New Phytol* **244**, 997-1012 (2024).
579
580 18. Yang C*, et al.* FgVps9, a Rab5 GEF, Is Critical for DON Biosynthesis and Pathogenicity in
581 Fusarium graminearum. *Front Microbiol* **11**, 1714 (2020).
582
583 19. Zheng W*, et al.* The endosomal recycling of FgSnc1 by FgSnx41-FgSnx4 heterodimer is
584 essential for polarized growth and pathogenicity in *Fusarium graminearum*. *New Phytol* **219**,
585 654-671 (2018).
586
587 20. Zheng W*, et al.* Retrograde trafficking from the endosome to the trans-Golgi network mediated
588 by the retromer is required for fungal development and pathogenicity in Fusarium graminearum.
589 *New Phytol* **210**, 1327-1343 (2016).
590
591 21. Wang S*, et al.* The regulatory role of the Aspergillus flavus core retromer complex in aflatoxin
592 metabolism. *J Biol Chem* **298**, 102120 (2022).
593
594 22. Xie Q*, et al.* ESCRT-III accessory proteins regulate fungal development and plant infection in
595 Fusarium graminearum. *Curr Genet* **65**, 1041-1055 (2019).

596
597 23. Xie Q, *et al.* Endosomal sorting complexes required for transport-0 is essential for fungal
598 development and pathogenicity in Fusarium graminearum. *Environ Microbiol* **18**, 3742-3757
599 (2016).
600
601 24. Xie Q, *et al.* Component interaction of ESCRT complexes is essential for endocytosis-
602 dependent growth, reproduction, DON production and full virulence in Fusarium graminearum.
603 *Front Microbiol* **10**, 180 (2019).
604
605 25. Sumarah MW. The deoxynivalenol challenge. *J Agric Food Chem* **70**, 9619-9624 (2022).
606
607 26. Abubakar YS, *et al.* FgRab5 and FgRab7 are essential for endosomes biogenesis and non-
608 redundantly recruit the retromer complex to the endosomes in Fusarium graminearum. *Stress*
609 *Biology* **1**, 1-12 (2021).
610
611 27. Zheng H, *et al.* Rab GTPases are essential for membrane trafficking-dependent growth and
612 pathogenicity in Fusarium graminearum. *Environmental Microbiology* **17**, 4580-4599 (2015).
613
614 28. Ekena K, Stevens TH. The Saccharomyces cerevisiae MVP1 gene interacts with VPS1 and is
615 required for vacuolar protein sorting. *Mol Cell Biol* **15**, 1671-1678 (1995).
616
617 29. Suzuki SW, Oishi A, Nikulin N, Jorgensen JR, Baile MG, Emr SD. A PX-BAR protein
618 Mvp1/SNX8 and a dynamin-like GTPase Vps1 drive endosomal recycling. *Elife* **10**, e69883
619 (2021).
620
621 30. Chi RJ, Liu J, West M, Wang J, Odorizzi G, Burd CG. Fission of SNX-BAR-coated endosomal
622 retrograde transport carriers is promoted by the dynamin-related protein Vps1. *J Cell Biol* **204**,
623 793-806 (2014).
624
625 31. Lou Y, *et al.* Genome-wide characterization of PX domain-containing proteins involved in
626 membrane trafficking-dependent growth and pathogenicity of Fusarium graminearum. *mBio* **12**,
627 e0232421 (2021).
628
629 32. Rojas R, *et al.* Regulation of retromer recruitment to endosomes by sequential action of Rab5
630 and Rab7. *J Cell Biol* **183**, 513-526 (2008).
631
632 33. Long Y, *et al.* Golgi-associated retrograde protein (GARP) complex recruits retromer to trans-
633 Golgi network for FgKex2 and FgSnc1 recycling, necessary for the development and
634 pathogenicity of Fusarium graminearum. *New Phytol* **246**, 666-688 (2025).
635
636 34. Gopaldass N, Chen KE, Collins B, Mayer A. Assembly and fission of tubular carriers mediating
637 protein sorting in endosomes. *Nat Rev Mol Cell Biol* **25**, 765-783 (2024).
638
639 35. Carosi JM, Denton D, Kumar S, Sargeant TJ. Receptor recycling by retromer. *Mol Cell Biol* **43**,

317-334 (2023).

36. Xu P, *et al.* COPI mediates recycling of an exocytic SNARE by recognition of a ubiquitin sorting signal. *Elife* **6**, e28342 (2017).

37. Chen SH, Shah AH, Segev N. Ypt31/32 GTPases and their F-Box effector Rcy1 regulate ubiquitination of recycling proteins. *Cell Logist* **1**, 21-31 (2011).

38. Henne WM, Buchkovich NJ, Emr SD. The ESCRT pathway. *Dev Cell* **21**, 77-91 (2011).

39. Ramachandran R, Schmid SL. The dynamin superfamily. *Curr Biol* **28**, R411-R416 (2018).

40. Daniel JA, *et al.* Phenothiazine-derived antipsychotic drugs inhibit dynamin and clathrin-mediated endocytosis. *Traffic* **16**, 635-654 (2015).

41. Grimsey EM, Piddock LJV. Do phenothiazines possess antimicrobial and efflux inhibitory properties? *FEMS Microbiol Rev* **43**, 577-590 (2019).

42. Morris GM, *et al.* AutoDock4 and AutoDockTools4: Automated docking with selective receptor flexibility. *J Comput Chem* **30**, 2785-2791 (2009).

43. Riquelme M. Tip growth in filamentous fungi: a road trip to the apex. *Annu Rev Microbiol* **67**, 587-609 (2013).

44. Ferguson SM, De Camilli P. Dynamin, a membrane-remodelling GTPase. *Nat Rev Mol Cell Biol* **13**, 75-88 (2012).

45. Antonny B, *et al.* Membrane fission by dynamin: what we know and what we need to know. *EMBO J* **35**, 2270-2284 (2016).

46. Zhong K, *et al.* MoDnm1 dynamin mediating peroxisomal and mitochondrial fission in complex with MoFis1 and MoMdv1 is important for development of functional appressorium in Magnaporthe oryzae. *PLoS Pathog* **12**, e1005823 (2016).

47. Kang J-b, *et al.* Mitochondrial dynamics caused by QoIs and SDHIs fungicides depended on FgDnm1 in Fusarium graminearum. *Journal of Integrative Agriculture* **22**, 481-494 (2023).

48. Chong X, *et al.* The dynamin-like GTPase FgSey1 plays a critical role in fungal development and virulence in Fusarium graminearum. *Appl Environ Microbiol* **86**, e02720-02719 (2020).

49. Arlt H, Reggiori F, Ungermann C. Retromer and the dynamin Vps1 cooperate in the retrieval of transmembrane proteins from vacuoles. *J Cell Sci* **128**, 645-655 (2015).

50. Ekal L, Alqahtani AMS, Hettema EH. The dynamin-related protein Vps1 and the peroxisomal

membrane protein Pex27 function together during peroxisome fission. *J Cell Sci* **136**, jcs246348 (2023).

51. Palmer SE*, et al.* A dynamin-actin interaction is required for vesicle scission during endocytosis in yeast. *Curr Biol* **25**, 868-878 (2015).

52. Ma M, Burd CG, Chi RJ. Distinct complexes of yeast Snx4 family SNX-BARs mediate retrograde trafficking of Snc1 and Atg27. *Traffic* **18**, 134-144 (2017).

53. Wu C*, et al.* The retromer CSC subcomplex is recruited by MoYpt7 and sequentially sorted by MoVps17 for effective conidiation and pathogenicity of the rice blast fungus. *Mol Plant Pathol* **22**, 284-298 (2021).

54. Bedsole CO, Vasselli JG, Shaw BD. Endocytosis in filamentous Fungi: Coordinating polarized hyphal growth and membrane recycling. *Fungal Genet Biol* **179**, 104000 (2025).

55. Weeratunga S, Paul B, Collins BM. Recognising the signals for endosomal trafficking. *Curr Opin Cell Biol* **65**, 17-27 (2020).

56. Wang J, Fedoseienko A, Chen B, Burstein E, Jia D, Billadeau DD. Endosomal receptor trafficking: Retromer and beyond. *Traffic* **19**, 578-590 (2018).

57. Jaszczyszyn A*, et al.* Chemical structure of phenothiazines and their biological activity. *Pharmacol Rep* **64**, 16-23 (2012).

58. Varga B, Csonka A, Csonka A, Molnar J, Amaral L, Spengler G. Possible biological and clinical applications of phenothiazines. *Anticancer Res* **37**, 5983-5993 (2017).

59. Sharma S, Kaur H, Khuller GK. Cell cycle effects of the phenothiazines: trifluoperazine and chlorpromazine in Candida albicans. *FEMS Microbiol Lett* **199**, 185-190 (2001).

60. Amaral L*, et al.* Phenothiazines, bacterial efflux pumps and targeting the macrophage for enhanced killing of intracellular XDRTB. *In Vivo* **24**, 409-424 (2010).

61. Cossart P, Helenius A. Endocytosis of viruses and bacteria. *Cold Spring Harb Perspect Biol* **6**, (2014).

62. Elwell C, Engel J. Emerging Role of Retromer in Modulating Pathogen Growth. *Trends Microbiol* **26**, 769-780 (2018).

63. Simonetti B, Daly JL, Cullen PJ. Out of the ESCPE room: Emerging roles of endosomal SNX-BARs in receptor transport and host-pathogen interaction. *Traffic* **24**, 234-250 (2023).

64. Yuen ELH, Shepherd S, Bozkurt TO. Traffic Control: Subversion of Plant Membrane

Trafficking by Pathogens. *Annu Rev Phytopathol* **61**, 325-350 (2023).

65. Chen X*, et al.* Trehalose phosphate synthase complex-mediated regulation of trehalose 6-phosphate homeostasis is critical for development and pathogenesis in Magnaporthe oryzae. *mSystems* **6**, (2021).

66. Jia LJ, Wang WQ, Tang WH. Wheat Coleoptile Inoculation by Fusarium graminearum for Large-scale Phenotypic Analysis. *Bio Protoc* **7**, e2439 (2017).

67. Schindelin J*, et al.* Fiji: an open-source platform for biological-image analysis. *Nat Methods* **9**, 676-682 (2012).

68. Letunic I, Bork P. Interactive Tree of Life (iTOL) v6: recent updates to the phylogenetic tree display and annotation tool. *Nucleic Acids Res*, (2024).

69. Mirdita M, Schutze K, Moriwaki Y, Heo L, Ovchinnikov S, Steinegger M. ColabFold: making protein folding accessible to all. *Nat Methods* **19**, 679-682 (2022).

764 **Figure legend**

765

766 **Fig.1 Rab GTPases FgRab51 and FgRab7 coordinate the intracellular dynamic of FgVps1**

767 A. Pathogenicity assay of the indicated strains on wheat heads. B. GFP-FgVps1 pull down strategy
768 for identification of putative FgVps1 interacting proteins. C. Co-IP assay verifying the interaction
769 of FgVps1 with the Rab GTPase FgRab51. D. Time-lapse imaging and motion trajectory analysis
770 of GFP-FgRab51 and mCherry-FgVps1. A total of 37 time-lapse images was taken at 1.64s interval.
771 Arrows indicate shared trafficking trajectory of FgVps1 and FgRab51. E. Co-IP assay verifying the
772 interaction of FgVps1 with the Rab GTPase FgRab7. F. Time-lapse imaging and motion trajectory
773 analysis of GFP-FgRab7 and mCherry-FgVps1. A total of 37 time-lapse images was taken at 1.29s
774 interval. Arrows indicate shared trafficking trajectory of FgVps1 and FgRab7. G. Statistical analysis
775 of the motion trajectories of FgVps1 in the wild type and Rab GTPase mutants (**P<0.01). The
776 time-lapse imaging involved a total of 150 images was taken at 200 ms interval. H. Fluorescence
777 recovery after photobleaching assay to analyze the fluorescence recovery rate of FgVps1 in the wild
778 type and Rab GTPase mutants.

779

780

781

782 **Fig. 2 Loss of *FgVPS1* compromises the proper sorting of FgSnc1**

783 A. Prosed model for FgSnx4-mediated FgSnc1 trafficking in *F. graminearum.* B. Analysis of the
784 vegetative growth, apical hyphal morphology and pathogenicity in the indicated strains. C. Time-
785 lapse imaging of GFP-FgSnc1 and mCherry-FgVps1 and analysis of their respective trajectory. A
786 total of 42 images was taken at 1.4s interval. D. Fluorescence recovery after photobleaching assay
787 for the fluorescence recovery rate of FgSnc1 in the wild type, Δ*Fgsnx4* and Δ*Fgvps1* mutants. E.
788 Microscopic observation and statistical analysis of FgSnc1 localization in the basal hyphae of the
789 wild type, Δ*Fgsnx4* and Δ*Fgvps1* mutants. To visualize the vacuolar lumen, the hyphae were stained
790 with CMAC dye. Localization differences were analyzed from 30 hyphae per biological replicate,
791 with three independent replicates involved (**P<0.01). F. Western blots for FgSnc1 degradation in
792 the wild type, Δ*Fgsnx4* and Δ*Fgvps1* mutants. For western blot analysis, the indicated fungal strains
793 were grown in CM liquid medium for 36 hours.

794

795

796

797 **Fig. 3 FgVps1 modulates the endosomal release of FgVps35 and FgSnx4**

798 A. Motion trajectory analysis of FgVps1 with FgSnx4 and FgVps35, as well as FgSnx4 with

FgVps35. A total of 36 images was taken at 1.6s interval. B. Venn diagram visualization of the interacting proteins of FgVps1, FgVps35 and FgSnx4. C. Time-lapse imaging and trajectory analysis of FgVps35 and FgSnx4 in the wild type and Δ*Fgvps1* mutant. A total of 45 images was taken at 1.3s interval. Arrows indicate speckled structures at the hyphal tips or elongated tubules in the basal hyphae as observed in the Δ*Fgvps1* mutant. D. Yeast two-hybrid assay confirming the interaction between FgVps35 and FgSnx4. E. Co-IP assay verifying the interaction between FgVps35 and FgSnx4. F. Yeast two-hybrid assay verifying the interaction sites of FgVps35 and FgSnx4. The interaction model of FgVps35 with the sorting nexin FgSnx4 was predicted by Alphafold2. FgVps35 is represented in light blue, FgSnx4 is represented in pale green. Black box indicates the zoomed area. Yellow dash represents the hydrogen bond formed between FgSnx4 E373 and FgVps35 N383. G. Analysis of the pathogenicity of the indicated strains on wheat spikes (**P<0.01).

Fig. 4 The ESCRT complex component FgVps36 contributes to the homeostasis of the endolysosomal network

A. Yeast two hybrid assay showing positive interaction between the ESCRT machinery and FgVps35 and FgSnx4. B. A simplified schematic showing the interaction among FgVps35, FgSnx4 and the related ESCRT complex components. C. CMAC staining for the observation of vacuole in the wild type and Δ*Fgvps36* mutant. D. Western blot assay for the detection of endosomal network components in the wild type and Δ*Fgvps36* mutant. For western blot assays, the indicated strains were cultured in liquid complete medium for 36 h for proteins extraction, and further enriched using GFP-trap beads. E and F. Effect of *FgVPS36* deletion on the intracellular homeostasis of FgVps35 and FgSnx4. For confocal imaging, the strains were cultured on complete medium for 2 days and then observed under a confocal microscope. Arrows indicate the co-localization of FgVps36 with FgVps35 or FgSnx4. Bar charts represent the quantitative data of the localization patters of FgVps35 and FgSnx4 in the wild type and Δ*Fgvps36* mutant. **P<0.01. G. Analysis of motion trajectory of FgVps36 with FgSnc1. A total of 12 frames was taken at 5.2-second intervals. Arrows indicate the shared trafficking trajectory of FgVps36 and FgSnc1. H. Analysis of motion trajectory of FgSnc1 in the wild type and Δ*Fgvps36* mutant. A total of 57 frames was taken at 500ms intervals. Black arrow indicates the movement of FgSnc1 at the hyphal tip. I. Confocal examination for the distribution of FgSnc1 in the basal hyphae of the wild type and Δ*Fgvps36* mutant. Vacuole were stained with CMAC dye, **P<0.01.

835

836 **Fig. 5 Inhibition of FgVps1 GTPase activity perturbs FgSnc1 sorting in *F. gramienarum***

837 A. Purification of GST and GST-FgVps1 recombinant proteins and further analysis of GTPase
838 activity. To evaluate the effects of phenothiazines on FgVps1 GTPase activity, 5 μL of the purified
839 GST-FgVps1 was incubated with 5 μL of phenothiazines (at a final concentration of 100 μg/mL) for
840 30 min and then used for GTPase activity assay. B. Time-lapse imaging and trajectory analysis for
841 the effect of phenothiazines treatment on FgVps1 distribution. For confocal examination, the strains
842 expressing GFP-FgRab7 and mCherry-FgVps1 was inoculated on SYM medium with or without
843 phenothiazines for 2 days. A total of 47 images was taken at 1.2s interval. White arrows indicate the
844 abnormal puncta detected in the cytosol. C. Time-lapse imaging and trajectory analysis for the effect
845 of phenothiazines treatment on FgSnc1 distribution. A total of 300 images was taken at 200ms
846 interval. White arrows indicate the dynamics of FgSnc1 at the hyphal tip. D. Phenotype assays for
847 the effects of FgVps1 domain deletions on fungal development and pathogenicity. E. GTPase
848 activity assays of FgVps1$^{\Delta POC}$. The concentration of the purified recombinant proteins was
849 quantified, and then 10 μL of each protein was used for further GTPase activity assay. F. Growth
850 assay of FgVps1$^{\Delta POC}$ strain on CM medium. G. Pathogenicity assays of FgVps1$^{\Delta POC}$ strain on wheat
851 heads. G. Confocal microscopy and western blot assays for the effect of FgVps1$^{\Delta POC}$ on FgSnc1
852 sorting (**P<0.01).

853

854

855

856 **Fig. 6 Treatment with phenothiazines disrupts actin organization in SPK**

857 A. Effect of phenothiazine treatment on actin organization at hyphal tip polarity (**P<0.01). To
858 evaluate the effect of phenothiazines on actin organization, the wild type strain expressing Lifeactin-
859 RFP was inoculated onto CM plates supplemented with or without phenothiazines (50 μg/mL) for
860 2 days (**P<0.01). For motion trajectory analysis, A total of 47 images was taken at 400ms interval.
861 B. FM4-64 staining for monitoring endocytosis following treatment with phenothiazines (50 μg/mL)
862 and Lat A (5 μg/mL). C. Confocal examination for the endocytosis of FgUapC under phenothiazine
863 and Lat A treatments. To induce the endocytosis of FgUapC, the wild type strain expressing GFP-
864 FgUapC was shifted from a urea-containing medium to an ammonium-rich medium (10 μM NH_4Cl)
865 for 3.5 hours. Phenothiazines and Lat A were used at final concentrations of 50 μg/mL and 5 μg/mL,
866 respectively. White arrows indicate the plasma membrane localization of FgUapC. D. Confocal
867 examination and motion trajectory analysis of the effects of Lat A treatment on FgVps1 dynamic. A
868 total of 29 images was taken at 1s interval. E. Confocal examination for the effect of CPZ treatment
869 on actin organization in *M. oryzae* (**P<0.01). To evaluate the effect of the phenothiazine derivative
870 CPZ on actin organization, the wild type strain (70-15) expressing Lifeactin-RFP was inoculated on

871 CM plates containing 50 μg/mL CPZ. F. Effects of phenothiazines treatment on the growth of the
872 indicated fungal pathogens.
873
874
875
876 **Fig. 7 Proposed model for FgVps1-associated endosomal sorting in *F. graminearum***
877 Through endocytosis, cargo proteins (e.g. FgSnc1) are internalized and delivered to endosomes,
878 where endosomal sorting is initiated. At the endosomes, sorting nexins and the retromer complex
879 recognize specific cargo proteins and facilitate the formation of endosomal tubules. During this
880 process, the ESCRT machinery interacts with the sorting nexins and the retromer to prevent
881 misrouting and premature degradation of the cargos. As endosomal tubules mature, Rab GTPases
882 recruit the dynamin-like GTPase to promote vesicles release. The released vesicles are then
883 trafficked to target membranes for subsequent recycling. Disruption of the endosomal sorting, either
884 by inhibition of FgVps1 function or disruption of actin organization, efficiently inhibit fungal
885 development and pathogenicity.
886

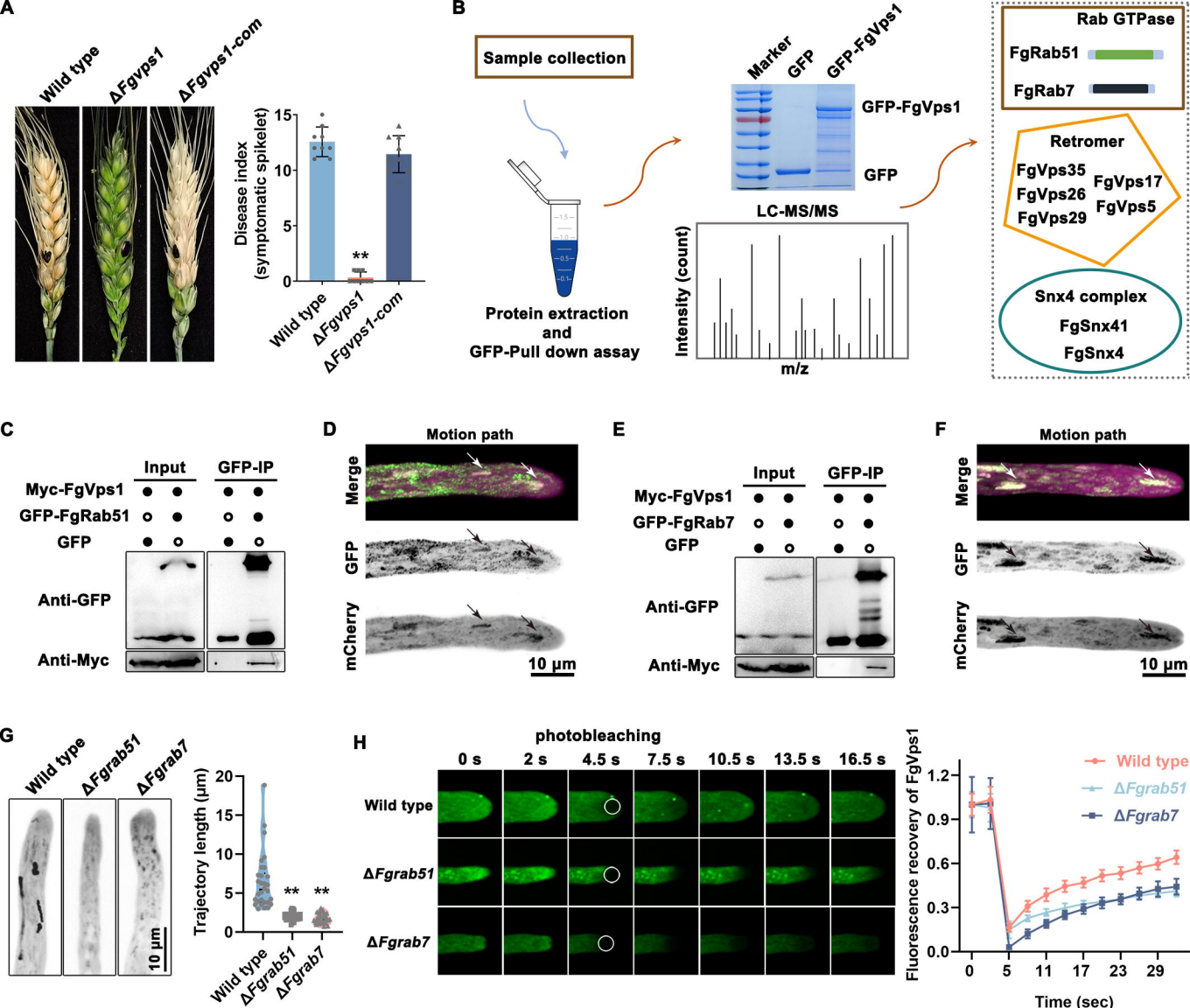
A
Wild type
ΔFgvps1
ΔFgvps1-com
Disease index (symptomatic spikelet)
15
10
5
0
**
Wild type
ΔFgvps1
ΔFgvps1-com
B
Sample collection
Protein extraction and GFP-Pull down assay
Marker
GFP
GFP-FgVps1
GFP-FgVps1
GFP
LC-MS/MS
Intensity (count)
m/z
Rab GTPase
FgRab51
FgRab7
Retromer
FgVps35
FgVps17
FgVps26
FgVps5
FgVps29
Snx4 complex
FgSnx41
FgSnx4
C
Input
GFP-IP
Myc-FgVps1
GFP-FgRab51
GFP
Anti-GFP
Anti-Myc
D
Motion path
Merge
GFP
mCherry
10 μm
E
Input
GFP-IP
Myc-FgVps1
GFP-FgRab7
GFP
Anti-GFP
Anti-Myc
F
Motion path
Merge
GFP
mCherry
10 μm
G
Wild type
ΔFgrab51
ΔFgrab7
10 μm
Trajectory length (μm)
20
15
10
5
0
**
**
Wild type
ΔFgrab51
ΔFgrab7
H
photobleaching
0 s
2 s
4.5 s
7.5 s
10.5 s
13.5 s
16.5 s
Wild type
ΔFgrab51
ΔFgrab7
Fluorescence recovery of FgVps1
1.2
0.9
0.6
0.3
0.0
0
5
11
17
23
29
Time (sec)
Wild type
ΔFgrab51
ΔFgrab7

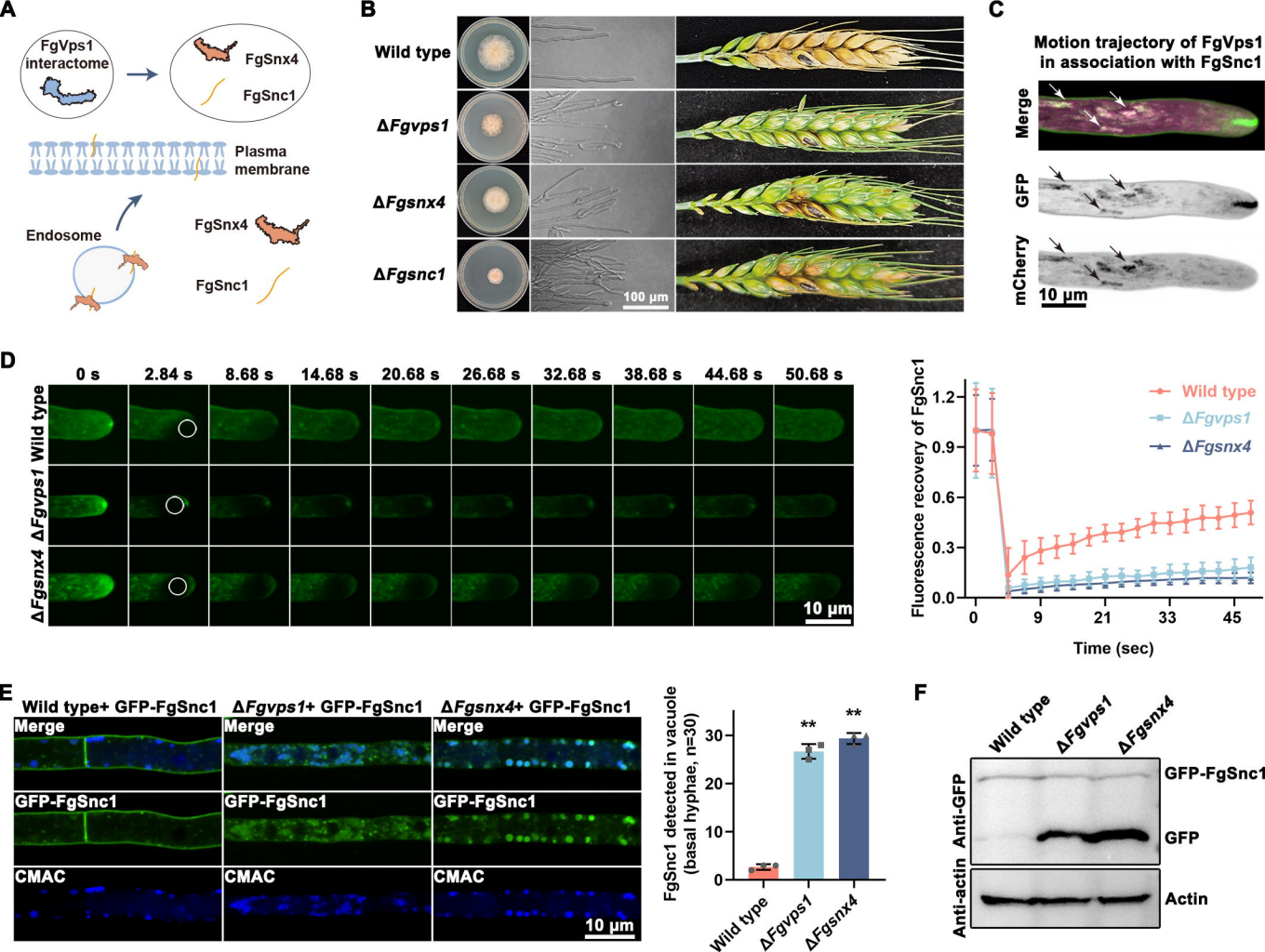
A
FgVps1 interactome
FgSnx4
FgSnc1
Plasma membrane
Endosome
FgSnx4
FgSnc1
B
Wild type
ΔFgvps1
ΔFgsnx4
ΔFgsnc1
100 μm
C
Motion trajectory of FgVps1 in association with FgSnc1
Merge
GFP
mCherry
10 μm
D
0 s
2.84 s
8.68 s
14.68 s
20.68 s
26.68 s
32.68 s
38.68 s
44.68 s
50.68 s
Wild type
ΔFgvps1
ΔFgsnx4
10 μm
Fluorescence recovery of FgSnc1
Wild type
ΔFgvps1
ΔFgsnx4
Time (sec)
E
Wild type+ GFP-FgSnc1
ΔFgvps1+ GFP-FgSnc1
ΔFgsnx4+ GFP-FgSnc1
Merge
GFP-FgSnc1
CMAC
10 μm
FgSnc1 detected in vacuole (basal hyphae, n=30)
Wild type
ΔFgvps1
ΔFgsnx4
F
Wild type
ΔFgvps1
ΔFgsnx4
Anti-GFP
GFP-FgSnc1
GFP
Anti-actin
Actin

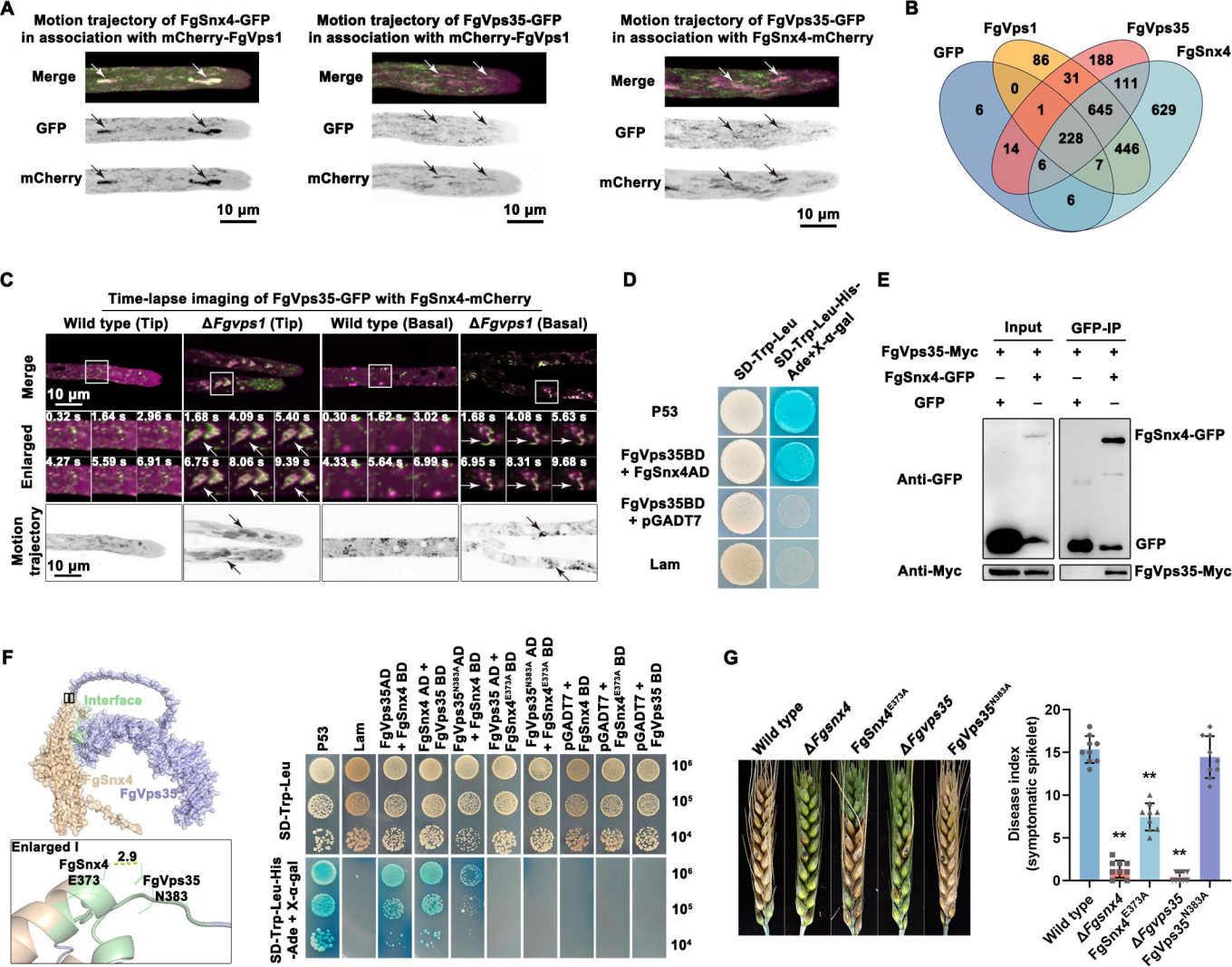
A
Motion trajectory of FgSnx4-GFP in association with mCherry-FgVps1
Motion trajectory of FgVps35-GFP in association with mCherry-FgVps1
Motion trajectory of FgVps35-GFP in association with FgSnx4-mCherry
Merge
GFP
mCherry
10 μm
B
FgVps1
FgVps35
GFP
FgSnx4
86
188
0
31
111
6
1
645
629
228
14
446
6
7
6
C
Time-lapse imaging of FgVps35-GFP with FgSnx4-mCherry
Wild type (Tip)
Δ*Fgvps1* (Tip)
Wild type (Basal)
Δ*Fgvps1* (Basal)
Merge
Enlarged
Motion trajectory
10 μm
0.32 s 1.64 s 2.96 s
1.68 s 4.09 s 5.40 s
0.30 s 1.62 s 3.02 s
1.68 s 4.08 s 5.63 s
4.27 s 5.59 s 6.91 s
6.75 s 8.06 s 9.39 s
4.33 s 5.64 s 6.99 s
6.95 s 8.31 s 9.68 s
D
SD-Trp-Leu
SD-Trp-Leu-His-Ade+X-α-gal
P53
FgVps35BD + FgSnx4AD
FgVps35BD + pGADT7
Lam
E
Input
GFP-IP
FgVps35-Myc
FgSnx4-GFP
GFP
Anti-GFP
Anti-Myc
FgSnx4-GFP
GFP
FgVps35-Myc
F
Interface
FgSnx4
FgVps35
Enlarged I
FgSnx4
E373
2.9
FgVps35
N383
P53
Lam
FgVps35AD + FgSnx4 BD
FgSnx4 AD + FgVps35 BD
FgVps35N383A AD + FgSnx4 BD
FgVps35 AD + FgSnx4E373A BD
FgVps35N383A AD + FgSnx4E373A BD
pGADT7 + FgSnx4 BD
pGADT7 + FgSnx4E373A BD
pGADT7 + FgVps35 BD
SD-Trp-Leu
SD-Trp-Leu-His -Ade + X-α-gal
10^6
10^5
10^4
G
Wild type
Δ*Fgsnx4*
FgSnx4E373A
Δ*Fgvps35*
FgVps35N383A
Disease index (symptomatic spikelet)
20
15
10
5
0
**
**
**
Wild type
ΔFgsnx4
FgSnx4E373A
ΔFgvps35
FgVps35N383A

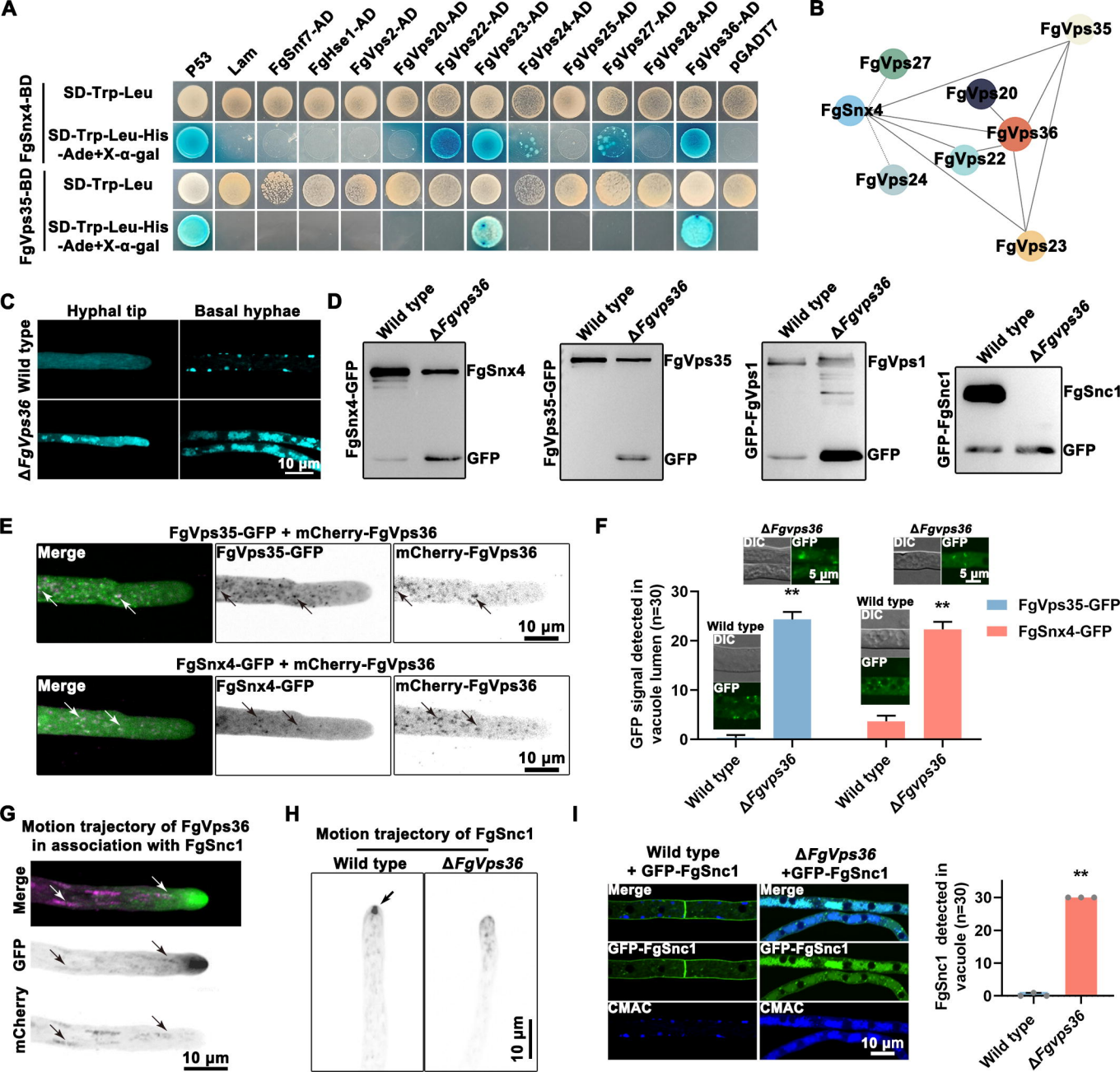
A
P53
Lam
FgSnf7-AD
FgHse1-AD
FgVps2-AD
FgVps20-AD
FgVps22-AD
FgVps23-AD
FgVps24-AD
FgVps25-AD
FgVps27-AD
FgVps28-AD
FgVps36-AD
pGADT7
FgSnx4-BD
SD-Trp-Leu
SD-Trp-Leu-His -Ade+X-α-gal
FgVps35-BD
SD-Trp-Leu
SD-Trp-Leu-His -Ade+X-α-gal
B
FgVps35
FgVps27
FgVps20
FgSnx4
FgVps36
FgVps22
FgVps24
FgVps23
C
Hyphal tip
Basal hyphae
Wild type
ΔFgVps36
10 μm
D
Wild type
ΔFgvps36
FgSnx4-GFP
FgSnx4
GFP
FgVps35-GFP
FgVps35
GFP
GFP-FgVps1
FgVps1
GFP
GFP-FgSnc1
FgSnc1
GFP
E
FgVps35-GFP + mCherry-FgVps36
Merge
FgVps35-GFP
mCherry-FgVps36
10 μm
FgSnx4-GFP + mCherry-FgVps36
Merge
FgSnx4-GFP
mCherry-FgVps36
10 μm
F
ΔFgvps36
DIC
GFP
5 μm
Wild type
GFP signal detected in vacuole lumen (n=30)
FgVps35-GFP
FgSnx4-GFP
**
Wild type
ΔFgvps36
G
Motion trajectory of FgVps36 in association with FgSnc1
Merge
GFP
mCherry
10 μm
H
Motion trajectory of FgSnc1
Wild type
ΔFgVps36
10 μm
I
Wild type + GFP-FgSnc1
ΔFgVps36 +GFP-FgSnc1
Merge
GFP-FgSnc1
CMAC
10 μm
FgSnc1 detected in vacuole (n=30)
**
Wild type
ΔFgvps36

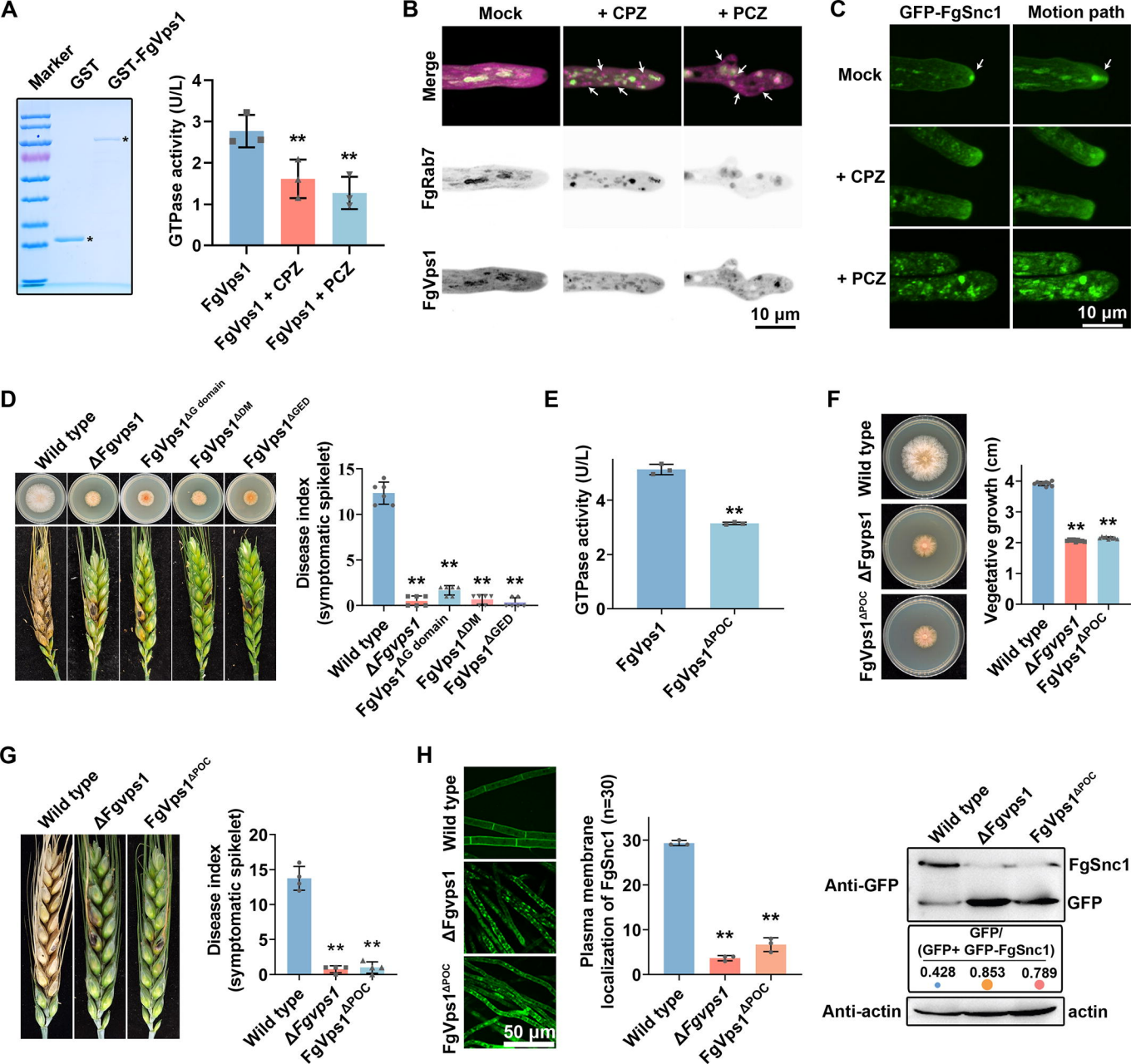
A
Marker
GST
GST-FgVps1
GTPase activity (U/L)
FgVps1
FgVps1 + CPZ
FgVps1 + PCZ
B
Mock
+ CPZ
+ PCZ
Merge
FgRab7
FgVps1
10 μm
C
GFP-FgSnc1
Motion path
Mock
+ CPZ
+ PCZ
10 μm
D
Wild type
ΔFgvps1
FgVps1ΔG domain
FgVps1ΔDM
FgVps1ΔGED
Disease index (symptomatic spikelet)
E
GTPase activity (U/L)
FgVps1
FgVps1ΔPOC
F
Wild type
ΔFgvps1
FgVps1ΔPOC
Vegetative growth (cm)
G
Wild type
ΔFgvps1
FgVps1ΔPOC
Disease index (symptomatic spikelet)
H
Wild type
ΔFgvps1
FgVps1ΔPOC
50 μm
Plasma membrane localization of FgSnc1 (n=30)
Anti-GFP
FgSnc1
GFP
GFP/ (GFP+ GFP-FgSnc1)
0.428
0.853
0.789
Anti-actin
actin

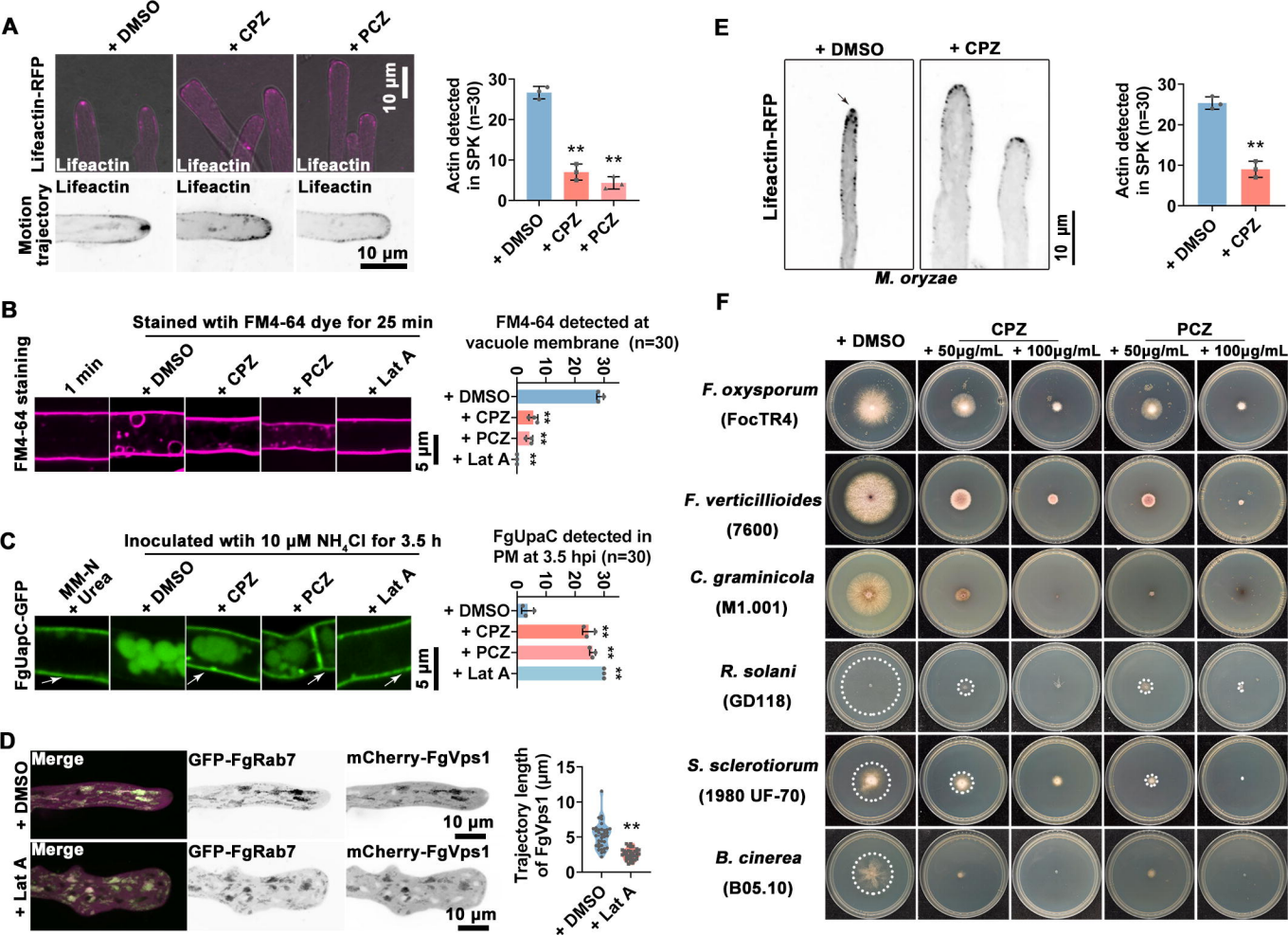
A
+ DMSO
+ CPZ
+ PCZ
Lifeactin-RFP
Lifeactin
10 μm
Motion trajectory
Actin detected in SPK (n=30)
**
B
Stained wtih FM4-64 dye for 25 min
FM4-64 staining
1 min
+ Lat A
5 μm
FM4-64 detected at vacuole membrane (n=30)
C
Inoculated wtih 10 μM NH4Cl for 3.5 h
MM-N + Urea
FgUapC-GFP
FgUpaC detected in PM at 3.5 hpi (n=30)
D
Merge
GFP-FgRab7
mCherry-FgVps1
Trajectory length of FgVps1 (μm)
E
M. oryzae
F
CPZ
PCZ
+ 50μg/mL
+ 100μg/mL
F. oxysporum (FocTR4)
F. verticillioides (7600)
C. graminicola (M1.001)
R. solani (GD118)
S. sclerotiorum (1980 UF-70)
B. cinerea (B05.10)

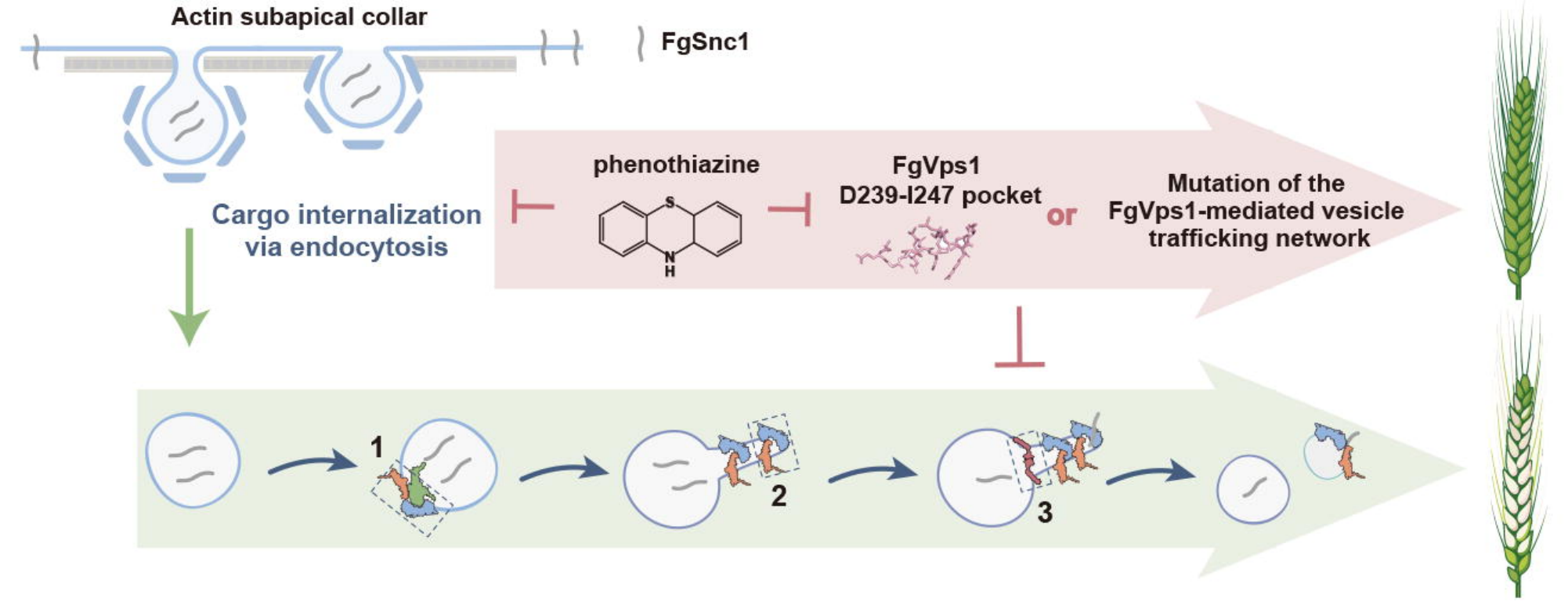
Actin subapical collar
FgSnc1
Cargo internalization via endocytosis
phenothiazine
S
N
H
FgVps1 D239-I247 pocket
or
Mutation of the FgVps1-mediated vesicle trafficking network
1
2
3

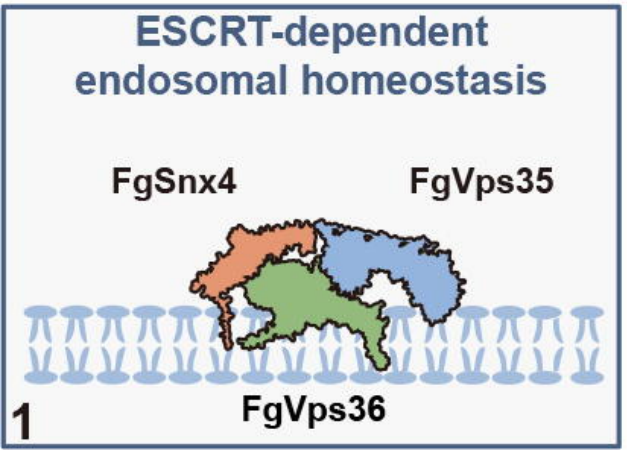
ESCRT-dependent endosomal homeostasis
FgSnx4
FgVps35
FgVps36
1

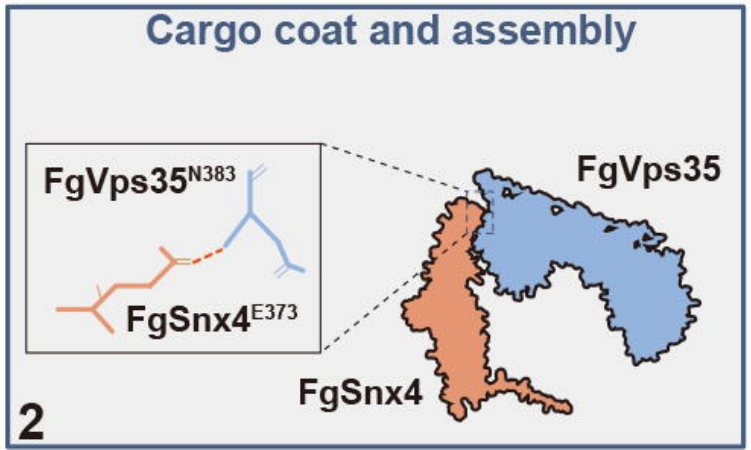
Cargo coat and assembly
FgVps35N383
FgSnx4E373
FgVps35
FgSnx4
2

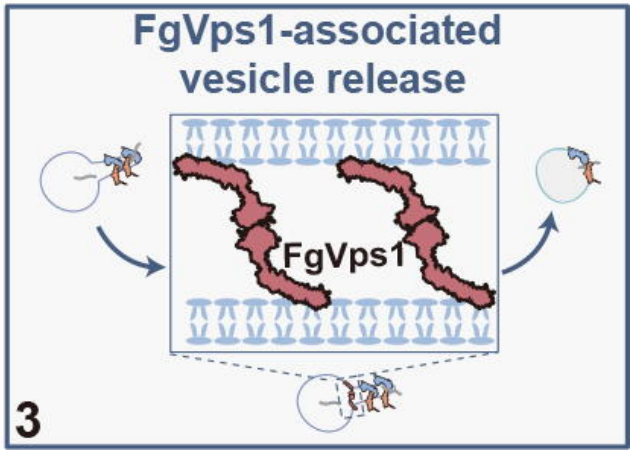
FgVps1-associated vesicle release
FgVps1
3